https://doi.org/10.22226/2410-3535-2022-2-169-174

Synthesis and characterization NS-reduced graphene oxide hydrogel and its electrochemical properties

A. Nugroho[†,1,2], F. Erviansyah[1], D. Floresyona[1,2], S. Mahalingam[3], A. Manap[3], N. Afandi[4], K. S. Lau[5], C. H. Chia[5]

[†]agung.n@universitaspertamina.ac.id

[1]Department of Chemical Engineering, Faculty of Industrial Technology, Universitas Pertamina, Jalan Teuku Nyak Arief, Simprug, Kebayoran Lama, Jakarta, 12220, Indonesia
[2]Center for Advanced Materials, Universitas Pertamina, Jalan Teuku Nyak Arief, Simprug, Kebayoran Lama, Jakarta, 12220, Indonesia
[3]Institute of Sustainable Energy, Universiti Tenaga Nasional, Jalan IKRAM-UNITEN, Kajang, Selangor, 43000, Malaysia
[4]Department of Mechanical Engineering, College of Engineering, Universiti Tenaga Nasional, Jalan IKRAM-UNITEN, Kajang, 43000, Malaysia
[5]Materials Science Program, Faculty of Science and Technology, Universiti Kebangsaan Malaysia, Bangi, Selangor, 43600, Malaysia

Developing materials with good electrochemical performance is critical in energy storage applications. One of the promising materials for these applications is reduced graphene oxide (rGO) based materials. Utilizing thiourea as a nitrogen (N) and sulfur (S) source, we present a simple hydrothermal approach for simultaneous doping of nitrogen and sulfur into the rGO hydrogel structure. The visual photograph shows the hydrogel form of the sample. XRD and Raman analysis shows the carbon structural changes during the reduction process. The presence of N and S atoms which spread evenly on the hydrogel structure, was confirmed by energy-dispersive x-ray (EDX) mapping. A cyclic voltammetry measurement at a current density of 0.5 A/g reveals that the NS-rGOH sample has a high specific capacity of 750 C/g. Even at a current density of 10 A/g, it can maintain outstanding charge-discharge stability, with 83.3% of the initial capacity preserved after 1000 charge-discharge cycles. Moreover, EIS analysis reveals that the low charge transfer resistance and high ionic diffusivity of the rGO hydrogel sample lead to good electrochemical performance. NS doping into the rGOH structure improves the sample's electrochemical performance compared to the undoped sample.

Keywords: doping, reduced graphene oxide, electrochemical, hydrothermal, supercapacitor.

1. Introduction

The rapidly expanding market for electronic devices and electric vehicles necessitates much work to improve energy storage technologies [1, 2]. Supercapacitors have the advantage over lithium-ion batteries due to their long cycle life, fast rate performance, high power density, and excellent safety [3]. Two types of principles in supercapacitors that have been studied widely are electrostatic double-layer capacitance (EDLC) and pseudocapacitance mechanism [4, 5]. EDLC mechanism occurs due to electrolyte-charge being physically absorbed in the surface of a conductive electrode. In contrast, in the pseudocapacitance mechanism an electron transfer reaction occurs at the electrode surface [6]. Based on these two mechanisms, the surface property of materials has a significant impact on their electrochemical properties when used as electrodes of supercapacitors [7].

Carbon-based materials such as mesoporous carbon, activated carbon, carbon nanotubes (CNT), or graphene are commonly used as an electrode in supercapacitors or lithium-ion batteries [7–12]. Amongst them, reduced graphene oxide (rGO) based materials have been widely studied due to their unique properties such as large surface area, high conductivity, and mechanical stability [11–14]. The current development of rGO-based EDLC has real capacitances in the 100–200 F/g range, much lower than the predicted theoretical value of 520 F/g [15]. Modifying the structure into hydrogel form can further improve the unique properties of rGO. Compared to powder form, rGO hydrogels have a larger surface area due to 3D porous structures, yet they do not aggregate significantly. The hydrothermal process reduces the functionalized graphene sheets by breaking oxygen-containing groups at high pressure and temperature, making it a viable strategy for large-scale graphene synthesis. The hydrothermal reduction process has various advantages over the chemical method, including ease of use, scalability, low defect content, and the ability to develop rGO in a more controlled fashion [16]. The structural stability and porosity of rGO hydrogel produced using the hydrothermal technique

make it suitable for energy storage applications [17]. Besides that, when the rGO hydrogel was applied as electrode's supercapacitors, the unique porous structure allowed for optimal electrolyte-electrode contact [18,19].

Sulfur, nitrogen, boron, fluorine, and other heteroatoms can be added to the rGO structure to alter its electrochemical characteristics [20–23]. Previous research shows that the addition of two heteroatoms simultaneously can be one of the strategy to improve the electrochemical performance of rGO in energy materials applications [24–26]. Due to the inclusion of pyrrole-N and pyridine-N, sulfone and sulfoxide group, nitrogen and sulfur (NS) co-doping on rGO leads to a distinctive electrical structure, defective morphology, and a sequence of redox faradic reactions [25]. As a result, the capacitive performance and surface wettability can be enhanced while charge transfer resistance can be suppressed [24–26].

This study uses a simple one-step hydrothermal technique to synthesize NS co-doped rGO hydrogel. The NS presence in the structure was characterized by Fourier Transform Infrared (FTIR) and scanning electron microscopy (SEM). The effect of two heteroatom doping inside the rGO structure results in different behavior in electrochemical properties. We use cyclic voltammetry (CV), galvanostatic charge-discharge (GCD) measurement, and Electrochemical Impedance Spectroscopy (EIS) to examine the electrochemical properties of the as-synthesized reduced graphene oxide materials.

2. Materials and experimental methods

2.1. Materials

Graphite flakes as the main precursor and thiourea (NH_2-CS-NH_2) as NS doping sources were obtained from Loba Chemie Pvt. Ltd. The necessary materials for oxidation of graphite such as sodium nitrate ($NaNO_3$), sulfuric acid (H_2SO_4) 98%, potassium permanganate ($KMnO_4$), hydrochloric acid (HCl) 37%, and hydrogen peroxide (H_2O_2) 30% were obtained from Smart Lab Indonesia Co. Ltd.

2.2. Preparation of Graphene Oxide

Graphene Oxide was prepared using modified Hummer's method from graphite flakes [27,28]. In 500 mL Erlenmeyer Flask, 2.0 g of graphite flakes and 2.0 g $NaNO_3$ and 90 mL concentrated H_2SO_4 were added and stirred while maintained at low temperature (0–5°C). Potassium permanganate (12.0 g) was slowly introduced into the suspension, kept the temperature under 15°C, and stirred for 4 hours. Distilled water (184.0 mL) was then added to the rest while mixing for 2 hours. Then the suspension was maintained at 98°C for 10 min before the decreasing temperature to 30°C until the color solution became brown. Further, 40.0 mL of H_2O_2 and 200.0 mL of H_2O were added and stirred for 1 h. It was then kept without stirring for 3 h until the slurry settled at the bottom to form a gel-like precipitate. The precipitate was washed by centrifugation using 10% HCl and distilled water at 7000 rpm at 10 minutes. This action repeats several times until reaching pH 7. The remaining slurry was then vacuum dried at 60°C for 6 h to produce GO powder.

2.3. Synthesis of reduced graphene oxide

An rGO sample was prepared by hydrothermal process from GO suspension with a 5 mg/mL concentration while rGOH used 8 mg/L. For NS-rGOH synthesis, 15 mL GO suspension and thiourea (1.8 g) were mixed and sonicated for 2 hours. The suspension was then undergoing hydrothermal synthesis at 180°C using 20 mL Teflon-lined autoclave [25]. The hydrothermal process lasted for 24 hours before naturally cooling down to room temperature. The remaining slurry was filtered and washed using distilled water and vacuum dried at 60°C for 2 hours.

2.4. Characterization

The presence of the functional group in the synthesized sample was examined using Fourier Transform Infrared (FTIR, Thermo Scientific Nicolet Spectrophotometer) in the spectrum range 500–4000 cm^{-1}. The solid-state crystallographic structure was determined by an X-ray diffractometer (XRD, Olympus BTX II Benchtop) using Co/Kα radiation. Defective morphology of the carbon structure in the sample was analyzed using Raman analysis (HORIBA — The LabRAM HR Evolution Raman Microscopes) measured in the range of 1000–2000 cm^{-1} using laser beam 532 nm and grating 1800 g/mm. The sample's morphologies and energy dispersive X-ray (EDX) spectra were verified using scanning electron microscopy (SEM) from Phenom ProX. The specific surface areas were investigated using Brunauer-Emmett-Teller technique (BET, JW-BK112, Surface Area Analyzer) during N_2 adsorption-desorption at 77 K.

2.5. Electrochemical measurement

The electrochemical performance of the synthesized samples was analyzed using a three-electrode system using Metrohm Autolab electrochemical instrument, with platinum serving as the counter electrode, and saturated calomel electrode (SCE) as the reference electrode. The working electrode was prepared by coating the sample ink into a glassy carbon electrode (0.07065 cm^2 area). The sample ink was prepared using the method described by Le et al., which included blending 2 mg of synthesized rGO sample with 1 ml of isopropanol and drying it in the open air for 10 minutes. After that, add 3 liters of Nafion and dry for 10 minutes in the open air [29]. All three-electrode was immersed in an electrolyte solution (6M KOH). CV measurement was tested in range potential window −1.25 until 0.25 V with various scan rates from 5 to 100 mV/s. EIS analysis was done in the range of 0.01 Hz to 100 kHz using AC voltage of 5 mV.

3. Results and discussion

FTIR spectroscopy is a widely known method that can be used to determine the functional group in the structure of carbon material. The FTIR spectra of the prepared GO, rGO, rGOH, and NS-rGOH, as well as graphite, are shown in Fig. 1a. The GO spectra show the peaks appeared at 3423, 1723, 1624, 1413, 1059 cm^{-1} which correspond to –OH, C=O

C=C, –C–OH, and –C–O– functional group, respectively. These appearances of oxide groups represent that the successful oxidation process of graphite. After the reduction process using hydrothermal synthesis, as shown by the rGO sample, the intensity descrease has been observed at 1723, 1626, and 1059 cm^{-1}, indicating the decomposition of the carboxyl group. The peak appearance at 1566 cm^{-1} confirmed the shifting of the C=C functional group of the sp^2 carbon network, which is usually found in other reduced graphene oxide samples [12, 30]. Further FTIR analysis of NS-rGOH shows the appearance of shoulders assigned to nitrogen and sulfur functional groups. The spectra show peaks at 3252, 1045, and 728 cm^{-1} corresponding to stretching N-H, bending C-N, and stretching C-S, respectively. This confirms that nitrogen and sulfur atom was successfully entered inside the rGO structure, which similar to the result of previous research [19, 24, 31].

The crystallographic and carbon structures of the synthesized rGO samples were identified using XRD and Raman analysis. The XRD patterns for graphite and as-synthesized samples are shown in Fig. 1b. Based on the XRD on (002) peak, the interlayer spacing of each sample was calculated using the Bragg equation [32, 33]. Graphite as starting material shows a diffraction peak at 26.58° with an interlayer spacing of 0.3351 nm. After the oxidation process, the graphitic peak shifts to the graphene oxide peak at 10.61°, increasing interlayer spacing to 0.8831 nm. This increase is because of layer stretching the penetration of oxygen compound in between graphite layer. After the hydrothermal reduction process, XRD patterns of rGO undergoing structural changes diffraction broad peak at $2\theta = 25.17°$ with interlayer spacing about 0.3535 nm suggest that reduction was successful. The addition of thiourea resulted in a larger layer interspacing (0.3651 nm). The NS-rGOH sample has interlayer spacing higher than rGOH indicate that exfoliation and reduction were successful and stretching occurs on the structure because of doping nitrogen and sulfur. After the reduction process, the loss of oxygen atoms was filled by N and S atoms in the crystal structure, affecting interlayer spacing [31]. The larger interlayer spacing could be the effect of the insertion of the large atomic size of sulfur atoms (0.102 nm) compared to carbon atoms (0.077 nm) [24].

Fig. 1c shows raman spectra of the as-synthesized samples in the range of 1000 to 2000 cm^{-1}. The spectra of graphite showed the D and G band peaks at 1344 and 1573 cm^{-1}, respectively. D band represents a defect on graphite structure due to doping atom or changes of carbon sp^2 to carbon sp^3. G band represents sp^2 carbon stretching vibration which is ordered graphitic structure on the carbon materials. Graphite samples show the I_D/I_G ratio about 0.152, which indicate that the graphite sample consists of a mainly ordered graphitic structure. The incorporation of the oxygen functional group on graphite lattice was confirmed by an increase in the intensity ratio from 0.152 to 0.944 for graphite and graphene oxide, respectively. The GO sample also shows broadening peaks on both the D and G bands compared to the graphite sample. This could be because of other defect structure presences in the GO sample. The successful reduction process is also shown by Raman spectra of rGO, which has a higher I_D/I_G value than the GO sample. There are significant differences between the I_D/I_G ratios of the as-synthesized samples. The hydrogel rGOH and NS-rGOH have a higher I_D/I_G than the rGO samples, which have a value of 1.019 and 1.012, respectively. These indicate that the introduction of S and N into hydrogel rGO layers causes more structural defects. Table S1 (Supplementary Material) presents the complete d-spacing and I_D/I_G ratio calculation result of each sample.

Clearly, from Fig. 2a, the NS-rGO sample shows the hydrogel structure. As comparison, the digital photograph of all synthesized sample also presented in Fig. S1 (Supplementary Material). This might be related to the optimum thiourea concentration, resulting in structural bonding with a water molecule to make a stable hydrogel structure. The SEM image of hydrogel rGO (Fig. 2b – c) shows an interconnected framework of nanosheets with a porous structure that can be seen in all samples. There is no observable change in the structure during the hydrothermal process of N and S doping. Fig. S2 (Supplementary Material). shows the comparison of the SEM image of rGO samples. BET surface area measurement results are 22.6, 75.21, and 59.96 m^2/g for rGO, rGOH and NS-rGOH samples. The result indicates that the surface area increased from rGO to rGOH samples due to hydrogel formation. After thiourea addition, the morphology results in similar hydrogel morphology with rGOH. However, NS doping into the rGO hydrogel structure results in decreasing surface area. EDX elemental mapping analysis in Fig. 2d – e suggest that mainly NS-rGOH samples

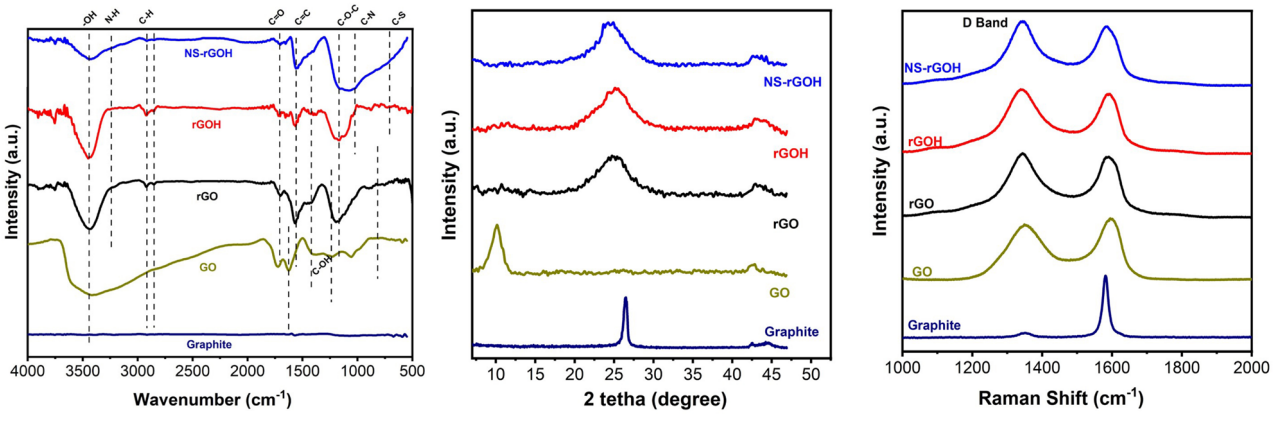

Fig. 1. (Color online) FTIR spectra (a), XRD pattern (b) and Raman spectra (c) of the synthesized samples.

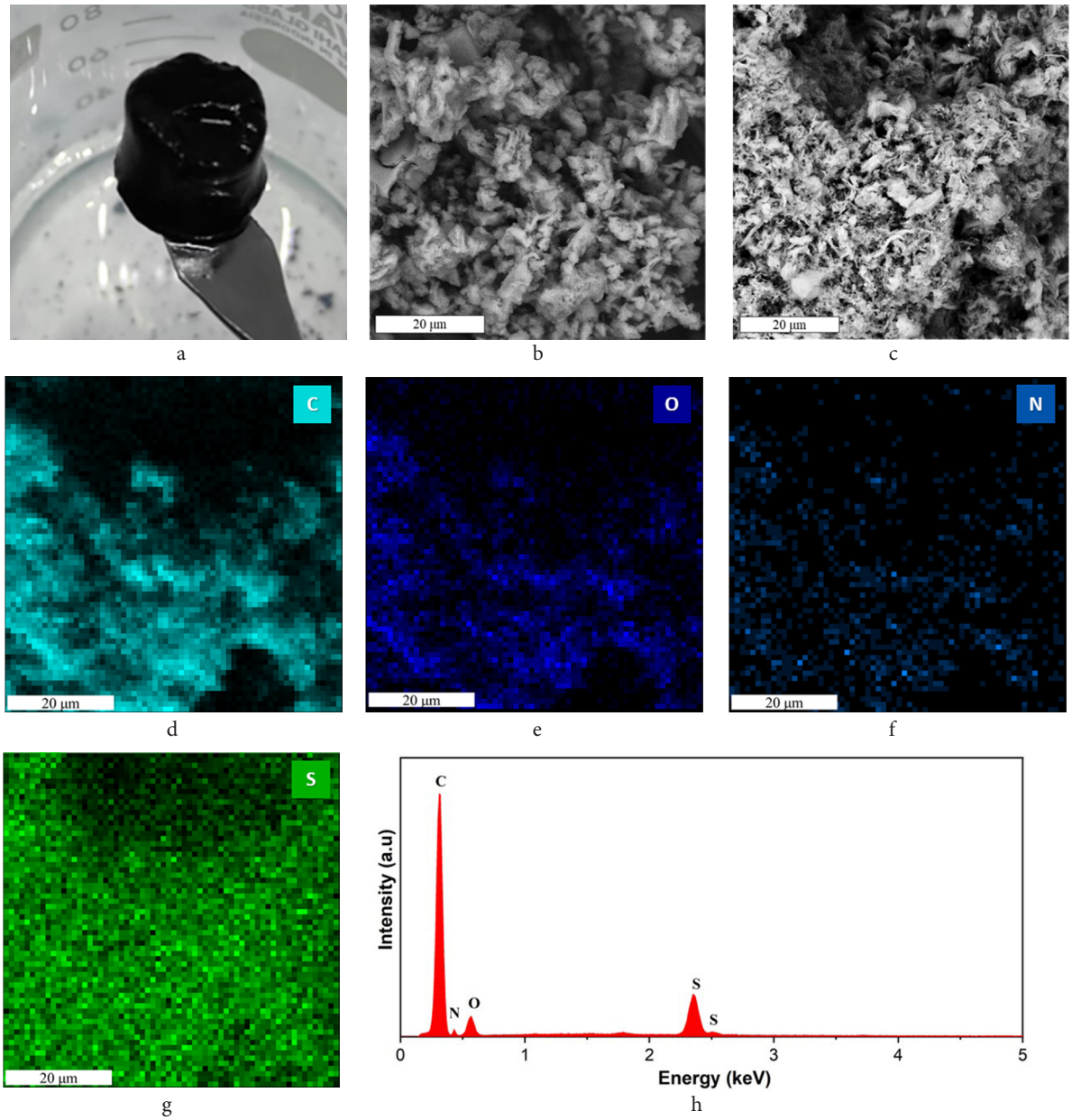

Fig. 2. (Color online) Digital photograph of NS-rGO hydrogel (a), SEM image of rGOH (b), NS-rGOH (c); and elemental mapping of NS-rGOH: carbon (d), oxygen (e), nitrogen (f), sulfur (g) and EDX spectra of NS-rGOH (h).

are composed of carbon (79.86 wt.%) with lower oxygen content (13.23 wt.%). This is common for reduced graphene oxide material having oxygen still attached to the graphene layer structure, as previously confirmed by FTIR analysis.

Furthermore, EDX data reveals that the sulfur and nitrogen weight content in NS-rGOH samples is 5.24% and 1.67%, respectively. Fig. 2 f and g show the good distribution detection elemental mapping of nitrogen and sulfur in the NS-rGOH structure. Fig. 2 h shows EDX spectra that confirm each element's presence in the NS-rGOH structure.

Cyclic voltammetry analysis of the synthesized rGO sample is shown in Fig. 3 a. CV curves of rGO samples suggest the electrical double layer capacitance (EDLC) behavior [30]. Meanwhile, the CV curve for NS-rGOH shows two peaks at −0.4 and −0.15 V, corresponding to the pseudocapacitance behavior. At scan rate of 20 mV/s, NS-rGOH shows a larger CV area compared to the rGOH and rGO sample. From the calculation of the curve area, NS-rGOH has a capacitance of 296.5 F/g, which is higher than rGO (115.1 F/g) and rGOH (118.4 F/g). This higher capacitance of NS-rGOH might be due to the redox peak shown at the CV curves, which means that a combination of EDLC and pseudocapacitance mechanism is responsible for the charge storage mechanism [25, 26]. The comparison of CV curve in various scan rates (Fig. S3, Supplementary Material) shows that the shape is consistent through all scan rate measurements.

We perform the GCD method at various current density to determine the electrochemical behavior of the as-synthesized materials. At a higher current density of 5 A/g (Fig. 3 b), the specific capacity of NS-rGOH calculated from GCD curves is 285 C/g which is significantly greater than rGO (35 C/g) and rGOH (100 C/g). This suggests that the hydrogel structure, larger specific surface area, and the NS doping effect are beneficial to improving the capacity. This result

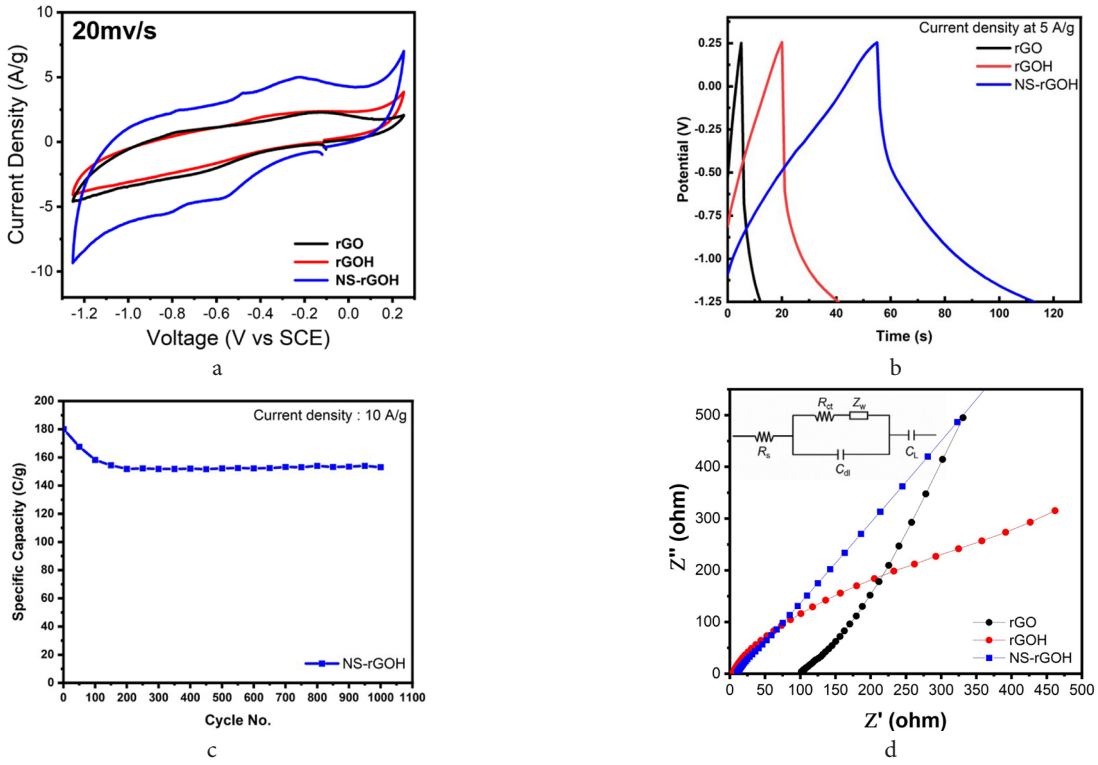

Fig. 3. (Color online) Cyclic Voltammetry curve at scan rate 20 mV/s (a), GCD measurement at 5 A/g (b), stability analysis (c), and EIS spectra of rGO, rGOH and NS-rGOH (d).

is also consistent when measurement performs at various current densities from 0.5 – 20 A/g (Fig. S4, Supplementary Material). The higher the current density, the faster the charge-discharge time. With increasing current density, the specific capacity shows a decreasing trend. It can be clearly seen that even at the highest current density of 20 A/g, the NS-rGOH has the highest capacity (120 C/g) compared to the rGO (2 C/g) and rGOH (20 C/g). The hydrogel structure has contributed higher capacity than the pristine rGO sample, which correlated with a higher surface area. Fig. 3c shows the stability of NS-rGOH at 10 A/g for 1000 cycles. The specific capacity of NS-rGOH decreases as the number of cycles increases. The result indicates that the NS-rGOH sample can retain 83% of the initial capacity even after 1000 cycles at a high current density (10 A/g). The comparison with other similar material also shows that our synthesized NS-rGO sample is comparable with similar graphene-based material in term of specific capacitance value as presented in Table S2 (Supplementary Material).

Electrochemical impedance spectroscopy Nyquist plots (Fig. 3 d) demonstrate the low equivalent series resistance in the high-frequency band (R_s). These plots also represent that the electrode material with the smaller semicircle in the mid-high frequency region has a lower charge transfer resistance (R_{ct}). The straight lines of NS-rGOH have good linearity and show a perfect capacitive characteristic at low frequencies regulated by diffusion. The resistance and diffusion phenomena can be evaluated using a corresponding equivalent circuit (inset Fig. 3 d). Simulated values of R_s and R_{ct} for rGO are 31.54 and 88.38 ohms, respectively. While for hydrogel samples, the series resistance was decreased to 22.75 ohms. The defect is due to NS doping on the structure, further lowering both resistance to 1.58 and 6.52 for R_s and R_{ct}, respectively. The low charge transfer resistance of NS-rGOH is probably due to the polarization increase of the carbon surface caused by NS doping. The diffusion coefficient calculation from the circuit model fitting of EIS for supercapacitor has previously done by Thalji et al. [34]. The calculation is based on the Warburg coefficient as a fitting result of the circuit model of the EIS analysis. The calculated diffusion coefficient (Table 1) of NS-doped reduced graphene oxide exhibits a higher diffusion coefficient than the undoped reduced graphene oxide (rGO and rGOH). This value indicates that the diffusivity ion of the NS-rGOH sample has increased due to NS doping on the hydrogel structure. The lower resistance and the high diffusivity of NS rGOH could be the reason for better electrochemical performance.

From the above analysis, NS doping is likely to cause structural defects in the graphene lattice, giving these materials a distinct electronic structure, a large specific surface area, and a large number of the active site. When nitrogen and sulfur are co-doped into rGO, it has a unique electronic structure and defected morphological characteristics which to pseudocapacitance mechanism. Even though BET surface area of NS-rGOH is lower than rGOH, the more active area due to NS defect on the surface can lead to higher electrochemical properties of NS-rGOH. This phenomenon is also similar with previous research in rGO doping. Lee et al show that

Table 1. Resistance and diffusivity coefficient calculated from EIS spectra of rGO, rGOH and NS-rGOH using the corresponding equivalent circuit.

Sample	R_s (ohm)	R_{ct} (ohm)	D_{K+} (cm^2/s)
rGO	31.54	88.38	4.14×10^{-14}
rGOH	22.75	0.76	4.09×10^{-14}
NS-rGOH	1.58	6.52	1.25×10^{-13}

the addition of B and N atom to the rGO structure led to the higher electrochemical properties even tough surface area is lower than the pristine rGO [35]. The pore size distributions of the synthesized rGO sample shown in Fig. S5 (Supplementary Material) show the different behavior of the pore distribution. The porous structure of NS-rGOH consisted of smaller porous structure compared to rGOH. The attachment of NS atom in the surface of rGO caused deterioration on the surface of rGO.

4. Conclusions

In conclusion, NS-rGOH was synthesized using a simple hydrothermal technique employing thiourea as a source of N, and S. The produced NS-rGOH had high porous structures and high surface area, which are advantageous for charge movement and ionic diffusion. Moreover, the NS-rGOH structure contains atoms N and S, which can significantly improve its electrochemical performance. At a current density of 0.5 A/g, it has a high specific capacity of 750 C/g. Even at a density of 10 A/g, it exhibits good charge- discharges stability with 83.3% of initial capacitance retention after 1000 cycles. Nitrogen and sulfur co-doped rGO with hydrogel structures is promising electrode material for high-rate performance supercapacitors.

Supplementary material. *The online version of this paper contains supplementary material available free of charge at the journal's Web site (lettersonmaterials.com).*

Acknowledgments. This research was supported by Universitas Pertamina and Universiti Tenaga Nasional (UNITEN) for funding this research under Universitas Pertamina-Uniten International Collaboration Grant of Grant No. 2020001YCUPU.

References

1. J. Wen, D. Zhao, C. Zhang. Renew. Energy. 162, 1629 (2020). Crossref
2. M. Horn, J. MacLeod, M. Liu, J. Webb, N. Motta. Econ. Anal. Policy. 61, 93 (2019). Crossref
3. S. Huang, X. Zhu, S. Sarkar, Y. Zhao. APL Mater. 7, 100901 (2019). Crossref
4. D. P. Chatterjee, A. K. Nandi. J. Mater. Chem. A. 9, 15880 (2021). Crossref
5. J. S. Ko, C.-H. Lai, J. W. Long, D. R. Rolison, B. Dunn, J. Nelson Weker. ACS Appl. Mater. Interfaces. 12, 20145 (2020). Crossref
6. Q. Li, M. Horn, Y. Wang, J. MacLeod, N. Motta, J. Liu. Materials. 12, 703 (2019). Crossref
7. B. You, F. Kang, P. Yin, Q. Zhang. Carbon. 103, 9 (2016). Crossref
8. M. Cossutta, V. Vretenar, T. A. Centeno, P. Kotrusz, J. McKechnie, S. J. Pickering. J. Clean. Prod. 242, 118468 (2020). Crossref
9. Z. Yang, J. Tian, Z. Yin, C. Cui, W. Qian, F. Wei. Carbon. 141, 467 (2019). Crossref
10. R. Dubey, V. Guruviah. Ionics (Kiel). 25, 1419 (2019). Crossref
11. D. Yoon, K. Y. Chung, W. Chang, S. M. Kim, M. J. Lee, Z. Lee, J. Kim. Chem. Mater. 27, 266 (2015). Crossref
12. E. Budi Nursanto, A. Nugroho, S.-A. Hong, S. J. Kim, K. Yoon Chung, J. Kim. Green Chem. 13, 2714 (2011). Crossref
13. E. I. Bîru, H. Iovu. In: Raman Spectrosc. Graphene Nanocomposites Studied by Raman Spectroscopy. (2018). Crossref
14. R. K. Mishra, G. J. Choi, Y. Sohn, S. H. Lee, J. S. Gwag. Chem. Commun. 56, 2893 (2020). Crossref
15. T. Wang, L. X. Wang, D. L. Wu, W. Xia, D. Z. Jia. Sci. Rep. 5, 1 (2015). Crossref
16. M. Ghorbani, H. Abdizadeh, M. R. Golobostanfard. Procedia Mater. Sci. 11, 326 (2015). Crossref
17. G. Gorgolis, C. Galiotis. 2D Mater. 4, 032001 (2017). Crossref
18. S. Han, D. Wu, S. Li, F. Zhang, X. Feng. Adv. Mater. 26, 849 (2014). Crossref
19. M. Abdul Mannan, Y. Hirano, A. T. Quitain, M. Koinuma, T. Kida. Micro Nanosyst. 12, 129 (2019). Crossref
20. K. Wang, L. Li, T. Zhang, Z. Liu. Energy. 70, 612 (2014). Crossref
21. F. Paquin, J. Rivnay, A. Salleo, N. Stingelin, C. Silva. J. Mater. Chem. C. 3, 10715 (2015). Crossref
22. T. Jin, J. Chen, C. Wang, Y. Qian, L. Lu. J. Mater. Sci. 55, 12103 (2020). Crossref
23. V. Thirumal, A. Pandurangan, R. Jayavel, R. Ilangovan. Synth. Met. 220, 524 (2016). Crossref
24. A. G. Kannan, J. Zhao, S. G. Jo, Y. S. Kang, D. W. Kim. J. Mater. Chem. A. 2, 12232 (2014). Crossref
25. W. Zhang, Z. Chen, X. Guo, K. Jin, Y. X. Wang, L. Li, Y. Zhang, Z. Wang, L. Sun, T. Zhang. Electrochim. Acta. 278, 51 (2018). Crossref
26. Z. Lu, Y. Chen, Z. Liu, A. Li, D. Sun, K. Zhuo. RSC Adv. 8, 18966 (2018). Crossref
27. B. Paulchamy, G. Arthi, B. D. Lignesh. J. Nanomed. Nanotechnol. 06, 1 (2015). Crossref
28. N. I. Zaaba, K. L. Foo, U. Hashim, S. J. Tan, W. W. Liu, C. H. Voon. Procedia Eng. 184, 469 (2017). Crossref
29. L. T. Le, M. H. Ervin, H. Qiu, B. E. Fuchs, W. Y. Lee. Electrochem. Commun. 13, 355 (2011). Crossref
30. K. Kakaei, A. Balavandi. J. Colloid Interface Sci. 490, 819 (2017). Crossref
31. R. A. Rochman, S. Wahyuningsih, A. H. Ramelan, Q. A. Hanif. IOP Conf. Ser. Mater. Sci. Eng. 509, 012119 (2019). Crossref
32. L. Stobinski, B. Lesiak, A. Malolepszy, M. Mazurkiewicz, B. Mierzwa, J. Zemek, P. Jiricek, I. Bieloshapka. J. Electron Spectros. Relat. Phenomena. 195, 145 (2014). Crossref
33. H. H. Huang, K. K. H. De Silva, G. R. A. Kumara, M. Yoshimura. Sci. Rep. 8, 2 (2018). Crossref
34. M. R. Thalji, G. A. M. Ali, P. Liu, Y. L. Zhong, K. F. Chong. Chem. Eng. J. 409, 128216 (2021). Crossref
35. J. W. Lee, T. Kshetri, K. R. Park, N. H. Kim, O.-K. Park, J. H. Lee. Compos. Part B Eng. 222, 109089 (2021). Crossref